9 MICRON CUTOFF 640 x 486 GaAs/$Al_xGa_{1-x}As$ QUANTUM WELL INFRARED PHOTODETECTOR SNAP-SHOT CAMERA

S. D. Gunapala, S. V. Bandara, J. K. Liu, W. Hong, M. Sundaram, P. D. Maker and R. E. Muller

Center for Space Microelectronics Technology, Jet Propulsion Laboratory,
California Institute of Technology, Pasadena, CA 91109

C.A. Shott, R. Carralejo,
Amber, A Raytheon Company, Goleta, CA 93117

ABSTRACT

A 9 μm cutoff 640x486 snap-shot quantum well infrared photodetector (QWIP) camera has been demonstrated. The performance of this QWIP camera is reported including indoor and outdoor imaging. Excellent imagery, with a noise equivalent differential temperature (NEΔT) of 36 mK has been achieved at 300 K background.

I INTRODUCTION

Quantum well infrared photodetectors (QWIPs) have achieved excellent imaging performance using large area 128x128 and 256x256 highly uniform focal plane arrays. Fabricated entirely from large bandgap materials which are easy to grow and process, it is now possible to obtain large uniform focal plane arrays (FPAs) of QWIPs tuned to detect light at wavelengths from 6 to 25 μm in the GaAs/Al_xGa_{1-x} As material system (1-4). Currently, there is a tremendous interest in long-wavelength QWIPs due to infrared (IR) imaging systems that require large area long-wavelength infrared (LWIR) focal

plane arrays for many applications, including night vision, navigation, flight control, early warning systems, Earth observing systems, astronomy, etc. Improving QWIP performance depends largely on minimizing the parasitic current that plagues all light detectors, the dark current (the current that flows through a biased detector in the dark, i.e., with no photons impinging on it) and improving the quantum efficiency. As we have discussed previously (1,5,6), at temperatures above 45 K, the dark current of the QWIPs having cutoff wavelengths in the 8-12 μm spectral region are entirely dominated by classic thermionic emission of ground state electrons into the energy continuum. Minimizing this dark current component is critical to the commercial success of the QWIP as it allows the highly-desirable 60-70 K operating temperature which can be easily achieved by single stage Stirling coolers.

In order to reduce this parasitic dark current, we have designed the bound-to-quasibound quantum well by placing the first excited state exactly at the well top. The previous QWIPs were called bound-to-continuum, because the first excited state was a continuum energy band above the well top (typically 10 meV). Dropping the first excited state to the well top causes the barrier to thermionic emission (roughly the energy height from the ground state to the well top) to be ~ 10 meV more in our bound-to-quasibound QWIP than in the bound-to-continuum one, theoretically causing the dark current to drop by a factor of ~ 6 at a temperature of 70 K (5-6). The dark current-voltage curve of the 8.3 μm peaked bound-to-quasibound QWIP is shown in Figure 1. This compares well with the factor of ~ 6 drop we have expected from the theoretical estimations.

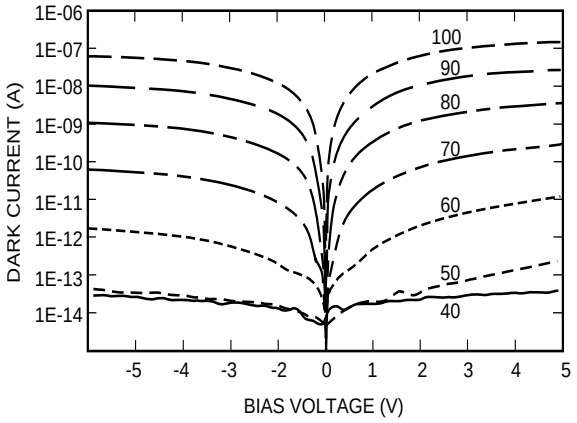

Figure 1. Dark current-voltage curves of 8.3 μm peaked bound-to-quasibound at temperatures from T = 40-100 K. Data were taken with a 200 μm diameter test structure and normalized to 18 x 18 μm² pixel.

II. TEST STRUCTURE RESULTS

A single period of the multi-quantum well (MQW) structure consists of a 45 Å well of GaAs (doped n ~ $5x10^{17}$ cm^{-3}) and a 500 Å barrier of $Al_{0.3}Ga_{0.7}As$. Stacking identical quantum wells (typically 50) together increases photon absorption. Ground state electrons are provided in the detector by doping the GaAs well layers with Si. This photosensitive MQW structure is sandwiched between 0.5 μm GaAs top and bottom contact layers doped n = $5x10^{17}$ cm^{-3}, grown on a semi-insulating GaAs substrate by molecular beam epitaxy (MBE). Then a 1.0 μm thick GaAs cap layer on top of a 300 Å $Al_{0.3}Ga_{0.7}As$ stop-etch layer was grown *in situ* on top of the device structure to fabricate the light coupling optical cavity. The MBE grown QWIP structure was processed into 200 μm diameter mesa test structures (area = 3.14 x 10^{-4} cm^2) using wet chemical etching, and Au/Ge ohmic contacts were evaporated onto the top and bottom contact layers.

The detectors were back illuminated through a 45° polished facet (5) and a responsivity spectrum is shown in Figure 2. The responsivity of the detector peaks at 8.3 μm and the peak responsivity (R_p) of the detector is 124 mA/W at bias V_B = -2 V. The spectral width and the cutoff wavelength are $\Delta\lambda/\lambda$ = 10% and λ_c = 8.8 μm respectively. The bias dependent peak responsivity of the detector was measured and it is small up to about V_B = -0.5 V. Beyond that it increases nearly linearly with bias reaching R_P = 179 mA/W at V_B = -5 V. This type of behavior of responsivity versus bias is typical for a bound-to-quasibound QWIP. The peak quantum efficiency was 17.5% at bias

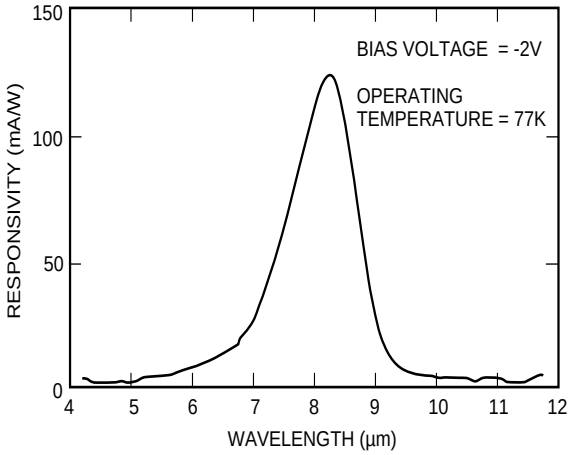

Figure 2. Responsivity spectrum of a bound-to-quasibound LWIR QWIP test structure at temperature T = 77 K. The spectral response peak is at 8.3 μm and the long wavelength cutoff is at 8.8 μm.

V_B = -2 V for a 45° double pass. The lower quantum efficiency is due to the lower well doping density ($5x10^{17}$ cm^{-3}) as it is necessary to suppress the dark current at the highest possible operating temperature. A peak quantum efficiency as high as 25% has already been achieved with regular well doping density (i.e., $1x10^{18}$ cm^{-3}). Due to lower readout multiplexer well depth (i.e., $9x10^6$ electrons) a lower dark current is mandatory to achieve a higher operating temperature. In this case, the highest operating temperature of 70 K was determined by the cooling capacity of the liquid nitrogen laboratory dewar. The operating temperature of 70 K has been achieved by pumping on liquid nitrogen.

The photoconductive gain g was experimentally determined using (5) $g = i_n^2 / 4eI_D B$, where B is the measurement bandwidth, and i_n is the current noise, which was measured using a spectrum analyzer. The photoconductive gain of the detector reached 0.98 at V_B =-5 V. The peak detectivity is defined as $D_P^* = R_P \sqrt{AB} / i_n$, where R_P is the peak responsivity. The measured peak detectivity at bias V_B = -3.0 V and temperature T = 70 K is $1.8x10^{11}$ cm $\sqrt{Hz}/W$. These detectors show background limited performance (BLIP) at bias V_B = -2 V and temperature T = 73 K for 300 K background with f/2 optics.

III. QWIP IMAGING FOCAL PLANE ARRAYS

Although random reflectors have achieved relatively high quantum efficiencies with large test device structures, it is not possible to achieve the similar high quantum efficiencies with random reflectors on small focal plane array pixels due to the reduced width-to-height aspect ratios. In addition, it is difficult to fabricate random reflectors for shorter wavelength detectors relative to very long-wavelength detectors (i.e., 15 μm) due to the fact that feature sizes of random reflectors are linearly proportional to the peak wavelength of QWIPs. For example, the minimum feature size of the random reflectors of 15 μm cutoff and 9 μm cutoff FPAs were 1.25 and 0.6 μm respectively and it is difficult to fabricate sub-micron features by contact photolithography. As a result,

the random reflectors of the 9 μm cutoff FPA were less sharp and had fewer scattering centers compared to the random reflectors of the 15 μm cutoff QWIP focal plane array It is well known that QWIPs do not absorb radiation incident normal to the surface unless the IR radiation has an electric field component normal to the layers of superlattice (growth direction) (5). As we have discussed before (5,8), more IR light can be coupled to the QWIP detector structure by incorporating a two dimensional grating surface on top of the detectors which also removes the light coupling limitations and makes two dimensional QWIP imaging arrays feasible. This two dimensional grating structure was fabricated on the detectors by using standard photolithography and CCl_2F_2 selective dry etching.

After the 2-D grating array was defined by the photolithography and dry etching, the photoconductive QWIPs of the 640x486 FPAs were fabricated by wet chemical etching through the photosensitive GaAs/$Al_xGa_{1-x}As$ multi-quantum well layers into the 0.5 μm thick doped GaAs bottom contact layer. The pitch of the FPA is 25 μm and the actual pixel size is 18x18 μm^2. The cross gratings on top of the detectors were then covered with Au/Ge and Au for Ohmic contact and reflection. Figure 3 shows twelve processed QWIP FPAs on a 3 inch GaAs wafer. Indium bumps were then evaporated on top of the detectors for Si readout circuit (ROC) hybridization. A single QWIP FPA was chosen and hybridized (via indium bump-bonding process) to a 640x486 direct injection silicon readout multiplexer (Amber AE-181) and biased at V_B = -2.0 V. Figure 4 shows a size comparison of this large area long-wavelength QWIP FPA to a quarter.

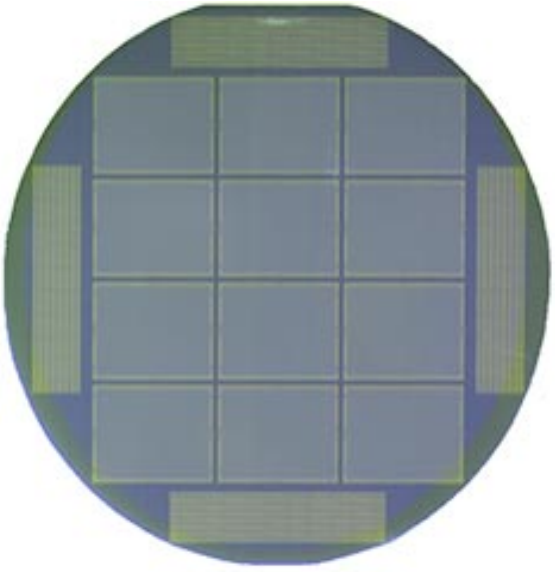

Figure 3. Twelve 640 x 486 QWIP focal plane arrays on a 3 in. GaAs wafer.

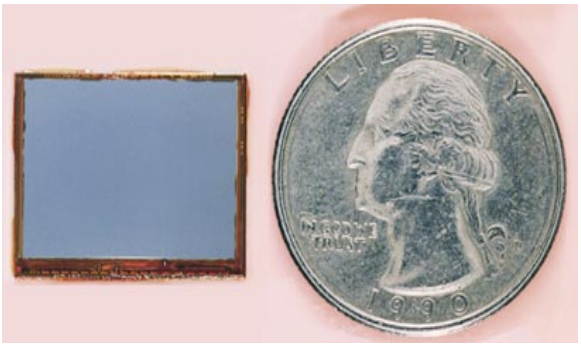

Figure 4. A size comparison of the 640 x 486 long-wavelength QWIP FPA to a quarter.

At temperatures below 70 K, the signal to noise ratio of the system is limited by array non-uniformity, multiplexer readout noise, and photo current (photon flux) noise. At temperatures above 70 K, temporal noise due to the QWIP's higher dark current becomes the limitation. As mentioned earlier this higher dark current is due to thermionic emission and thus causes the charge storage capacitors of the readout circuitry to saturate. Since the QWIP is a high impedance device, it should yield a very high charge injection coupling efficiency into the integration capacitor of the multiplexer. In fact Bethea *et al*. (2) have demonstrated charge injection efficiencies approaching 90%. Charge injection efficiency can be obtained from (3)

$$\eta_{inj} = \frac{g_m R_{Det}}{1 + g_m R_{Det}} \left[\frac{1}{1 + \frac{j\omega C_{Det} R_{Det}}{1 + g_m R_{Det}}} \right] \qquad (1)$$

where g_m is the transconductance of the MOSFET and is given by $g_m = eI_{Det}/kT$. The differential resistance R_{Det} of the pixels at -2 V bias is 5.4×10^{10} Ohms at T=70 K and detector capacitance C_{Det} is 1.4×10^{-14} F. The detector dark current I_{Det} = 24 pA under the same operating conditions. According to equation (1) the charge injection efficiency η_{inj}=99.5% at a frame rate of 30 Hz. The FPA was back- illuminated through the flat thinned substrate membrane (thickness $\approx$1300 Å). This thinned GaAs FPA membrane has completely eliminated the thermal mismatch between the silicon CMOS readout multiplexer and the GaAs based QWIP FPA. Basically, the thinned GaAs based QWIP FPA membrane adapts to the thermal expansion and contraction coefficients of the silicon readout multiplexer. Therefore, this thinning has played an extremely

important role in the fabrication of large area FPA hybrids. In addition, this thinning has completely eliminated the pixel-to-pixel optical cross-talk of the FPA. This initial array gave excellent images with 99.9% of the pixels working, demonstrating the high yield of GaAs technology. The operability was defined as the percentage of pixels having noise equivalent differential temperature less than 100 mK at 300 K background and in this case operability happens to be equal to the pixel yield.

We have used the following equation to calculate the noise equivalent temperature difference (NEΔT) of the FPA.

$$NE\Delta T = \frac{\sqrt{AB}}{D_B^*(dP_B / dT)\sin^2(\theta / 2)} \qquad (2)$$

where D_B^* is the blackbody detectivity, dP_B / dT is the derivative of the integrated blackbody power with respect to temperature, and θ is the field of view angle [i.e., $\sin^2(\theta/2) = (4f^2+1)^{-1}$, where f is the f number of the optical system]. The background temperature T_B = 300 K, the area of the pixel A = (18 μm)^2, the f number of the optical system is 2.3, and the frame rate is 30 Hz. Figure 5 shows the experimentally measured NEΔT of the FPA at an operating temperature of T = 70 K, bias V_B

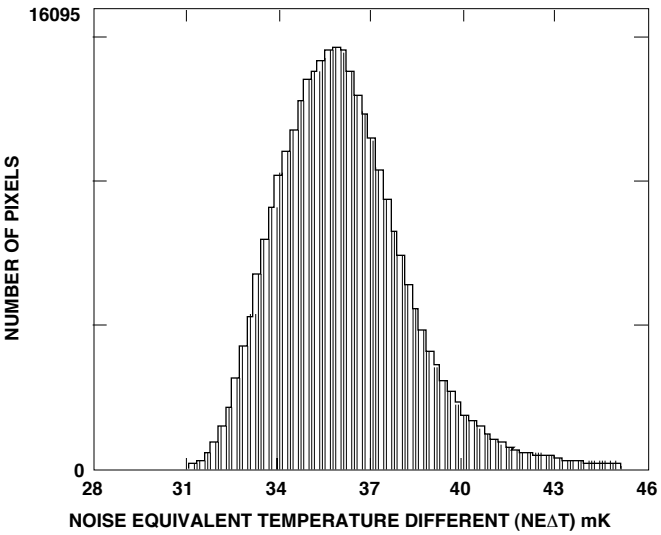

Figure 5. Noise equivalent temperature difference (NEΔT) histogram of the 311,040 pixels of the 640 x 486 array showing a high uniformity of the FPA. The uncorrected non-uniformity (= standard deviation/mean) of this unoptimized FPA is only 5.6% including 1% non-uniformity of ROC and 1.4% non-uniformity due to the cold-stop not being able to give the same field of view to all the pixels in the FPA.

= -2 V at 300 K background and the mean value 36 mK. This agrees reasonably with our estimated value of 25 mK based on test structure data. The experimentally measured peak quantum efficiency of the FPA was 2.3% (lower focal plane array quantum efficiency is attributed to 51% fill factor and 30% reflection loss from the GaAs back surface). Therefore, the corrected quantum efficiency of a focal plane detectors is 6.5% and this corresponds to an average of two pass of IR radiation (equivalent to a single 45˚ pass) through the photosensitive multi-quantum well region.

IV FOCAL PLANE ARRAY CAMERA

A 640X486 QWIP FPA hybrid was mounted onto a 84-pin lead-less chip carrier and installed into a laboratory dewar which is cooled by liquid nitrogen to demonstrate a LWIR imaging camera (shown in Figure 6). The other element of the camera is a 100 mm focal length AR coated germanium lens, which gives a 9.2˚x6.9˚ field of view. It is designed to be transparent in the 8-12 μm wavelength range to be compatible with the QWIP's 8-9 μm operation. The digital data acquisition resolution of the camera is 12-bits, which determines the instantaneous dynamic range of the camera (i.e., 4096), however, the dynamic range of QWIP is 85 Decibels.

Figure 6. Picture of the 640 x 486 long-wavelengths QWIP camera.

The measured mean NEΔT of the QWIP camera is 36 mK at an operating temperature of T = 70 K and bias V_B = -2 V at 300 K background. The uncorrected

NEΔT non-uniformity (which includes a 1% non-uniformity of the ROC and a 1.4% non-uniformity due to the cold-stop in front of the FPA not yielding the same field of view to all the pixels) of the 311,040 pixels of the 640x486 FPA is about 5.6% (= sigma/ mean). Figure 7 shows the noise histogram of this first unoptimized 640x486 QWIP FPA and the higher sigma/mean was due to the reduced number of samples acquired during the measurement. The non-uniformity after two-point (17˚ and 27˚ Celsius) correction improves to an impressive 0.1%. As mentioned earlier, this high yield is due to the excellent GaAs growth uniformity and the mature GaAs processing technology.

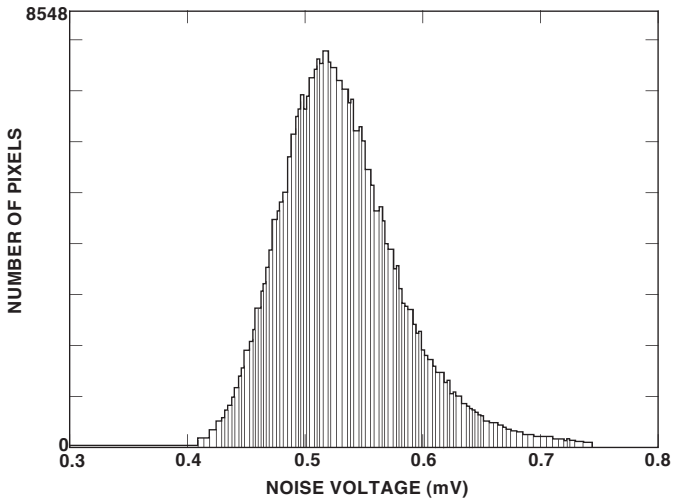

Figure 7. Noise histogram of the 640 x 486 long-wavelength QWIP FPA. The noise uniformity of this first unoptimized FPA is about 11% before corrections. It should be noted that these initial unoptimized FPA results are far from optimum.

Video images were taken at a frame rate of 30 Hz at temperatures as high as T = 70 K using a ROC capacitor having a charge capacity of $9x10^6$ electrons (the maximum number of photoelectrons and dark electrons that can be counted in the integration time of each detector pixel). Figure 8 (a) and (b) show two frames of video image taken with this long-wavelength 640x486 QWIP camera. The image in Figure 8(a) was taken in the night (around midnight) and it clearly shows where automobiles were parked during the day time. This image demonstrates the high sensitivity of the 640 x 486 long-wavelength QWIP staring array camera. Figure 8(b) show blades of a fast turning chopper wheel. The sharp straight edges of the chopper wheel demonstrate the snap-shot mode of operation.

(a)  (b) 

Figure 8(a), this picture was taken in the night (around midnight) and it clearly shows where automobiles were parked during the day time. This image demonstrates the high sensitivity of the 640 x 486 long-wavelength QWIP staring array camera. Figure 8(b) show blades of a fast turning chopper wheel. The sharp straight edges of the chopper wheel demonstrate the snap-shot mode of operation.

It should be noted that these initial unoptimized FPA results are far from optimum. The light coupling gratings were not optimized (as described earlier) for maximum light coupling efficiency, no anti-reflection coatings were used on the backside of the FPA, and finally the multiplexer used was not optimized to supply the proper bias required by photoconductive QWIPs (i.e., AE-181 was optimized for photovoltaic InSb FPAs). Implementation of these improvements should significantly enhance the QWIP FPA operating temperature (i.e., 77 K for 9 μm).

ACKNOWLEDGMENTS

The research described in this paper was performed by the Center for Space Microelectronics Technology, Jet Propulsion Laboratory, California Institute of Technology, and was jointly sponsored by the JPL Director's Research and Development Fund, the Ballistic Missile Defense Organization / Innovative Science & Technology Office, and the National Aeronautics and Space Administration, Office of Space Science.

REFERENCES

1. Sarath D. Gunapala, John K. Liu, Jin S. Park, Mani Sundaram, Craig A. Shott, Ted Hoelter, True-Lon Lin, S. T. Massie, Paul D. Maker, Richard E. Muller, and Gabby Sarusi" 9 μm Cutoff 256x256 GaAs/$Al_xGa_{1-x}As$ Quantum Well Infrared Photodetector Hand-Held Camera", IEEE Trans. Electron Devices, **44**, pp. 51-57, 1997.

2. C. G. Bethea, B. F. Levine, M. T. Asom, R. E. Leibenguth, J. W. Stayt, K. G. Glogovsky, R. A. Morgan, J. D. Blackwell, and W. J. Parrish, "Long Wavelength Infrared 128 x 128 AlxGa1-xAs/GaAs Quantum Well Infrared Camera and Imaging System," *IEEE Trans. Electron. Devices*, vol. 40, pp. 1957-1963, 1993.

3. L. J. Kozlowski, G. M. Williams, G. J. Sullivan, C. W. Farley, R. J. Andersson, J. Chen, D. T. Cheung, W. E. Tennant, and R. E. DeWames, "LWIR 128x128 GaAs/AlGaAs Multiple Quantum Well Hybrid Focal Plane Array," *IEEE Trans. Electron. Devices* , vol. ED-38, pp. 1124-1130, 1991.

4. W. A. Beck, T. S. Faska, J. W. Little, J. Albritton, and M. Sensiper, *Proceedings of the Second International Symposium on 2-20 μm Wavelength Infrared Detectors and Arrays: Physics and Applications*, October 10-12, 1994, Miami Beach, Florida.

5. S. D. Gunapala and K. M. S. V. Bandara, Physics of Thin Films, Academic Press, **21**, 113 (1995).

6. Sarath D. Gunapala, Jin S. Park, Gabby Sarusi, True-Lon. Lin, John K. Liu, Paul D. Maker, Richard E. Muller, Craig A. Shott, and Ted Hoelter, "15 μm 128x128 GaAs/AlGaAs Quantum Well Infrared Photodetector Focal Plane Array Camera", IEEE Trans. Electron Devices, **44**, pp. 45-50, 1997.

7. G. Sarusi, B. F. Levine, S. J. Pearton, K. M. S. V. Bandara, and R. E. Leibenguth, "Improved performance of quantum well infrared photodetectors using random scattering optical coupling," *Appl. Phys. Lett.*, vol. 64, pp. 960-962, 1994.

8. Sumith Bandara, Sarath Gunapala, John Liu, Winn Hong and Jin Park, "Optical coupling mechanisms in quantum well infrared photodetectors", Photodetectors; Materials and Devices, G. Brown and M. Razeghi, editor, Proc. SPIE **2999** (1997).